Journal of Non-Crystalline Solids 549 (2020) 120354

Contents lists available at ScienceDirect

Journal of Non-Crystalline Solids

journal homepage: www.elsevier.com/locate/jnoncrysol

Effect of Yttrium addition on magnetocaloric properties of Gd-Co-Al-Ho high entropy metallic glasses

C.M. Pang[a], C.C. Yuan[a,*], L. Chen[a], H. Xu[a], K. Guo[a], J.C. He[a], Y. Li[a], M.S. Wei[a], X.M. Wang[b], J.T. Huo[b], B.L. Shen[a,*]

[a] School of Materials Science and Engineering, Jiangsu Key Laboratory for Advanced Metallic Materials, Southeast University, Nanjing 211189, China
[b] CAS Key Laboratory of Magnetic Materials and Devices, Ningbo Institute of Materials Technology & Engineering, Chinese Academy of Sciences, Ningbo, Zhejiang 315201, China

ARTICLE INFO

Keywords:
Yttrium
High-entropy alloys
Magnetocaloric effect
Magnetic refrigeration
Metallic glasses

ABSTRACT

The $Gd_{25}Co_{25}Al_{25}Ho_{25-x}Y_x$ (x = 1, 5, 10, and 15) high entropy metallic glasses are fabricated by copper-mold quenching technique. Substituting moderately Ho with Y effectively improves the glass-forming ability, magnetic entropy change ($|\Delta S_M|$), and magnetic refrigeration capacity (RC) of $Gd_{25}Co_{25}Al_{25}Ho_{25-x}Y_x$. Besides, the Curie temperature of this quaternary alloy can be tuned from 51 to 41 K with Y addition. Among these alloys, $Gd_{25}Co_{25}Al_{25}Ho_{20}Y_5$ exhibits the largest peak value of $|\Delta S_M|$ up to 8.79 J kg^{-1}K^{-1} and the corresponding RC up to 547 J kg^{-1} under a magnetic field of 5 T. It is worthy to note that a reverse changing trend can be observed between the maximum $|\Delta S_M|$ and the temperature range of magnetic transition, which may be ascribed to the spatial inhomogeneity induced by yttrium microalloying. Our studies show that yttrium is an effective element to manipulate magnetocaloric properties of high entropy metallic glasses as potential refrigerants.

1. Introduction

Refrigeration is the process of cooling or freezing for preservative purposes by the various refrigerating machines and materials [1]. The traditional gas compression technology has been demonstrated that has many disadvantages, e.g., high energy loss, low efficiency, and environmental pollution [2,3]. Thus, the magnetic refrigeration attracts substantial attention due to its high efficiency and environmental friendliness [4,5]. The magnetic refrigeration cycle expels and absorbs heat by magnetization and demagnetization processes based on the magnetocaloric effect (MCE) that is as an inherent nature for magnetic materials [6]. Rare earth (RE) based alloys invariably exhibit excellent magnetocaloric properties due to its complex electronic structure and significant MCE [1,7,8]. It is generally accepted that RE-based magnetic refrigerants on the basis of its structure could be devided into crystalline and glassy refrigerants according to previous studies [9-11]. There are three main key parameters to evaluate the magnetocaloric properties of these refrigerants that are Curie temperature (T_C), magnetic entropy change($|\Delta S_M|$), and temperature range of magnetic transition (δT_{FWHM}) [12]. The crystalline refrigerant always possesses high magnetic transition temperature and gaint MCE, e.g. Gd-Si-Ge system, thus exhibits large T_C and $|\Delta S_M|$ [13]. However, its δT_{FWHM} is always very narrow due to the first-order magnetic phase change with the structure transition [14,10], which leads to the low refrigeration capacity calculated by the product of $|\Delta S_M|$ and δT_{FWHM}. As a result, the RE-based metallic glasses (MGs) have been explored due to their wide δT_{FWHM}. The $Gd_{55}Co_{20}Al_{25}$ bulk MG with a second-order magnetic phase change exhibits the relatively wider δT_{FWHM} up to 61.5 K than that of 16.4 K in the $Gd_5Si_2Ge_2$ alloy [15,13]. Moreover, the new alloy design concept of high entropy (HE) may extend the δT_{FWHM} by increasing mixed entropy that can restrain the rearrangement of magnetic monment in RE-based MG refrigerants [16].

The RE-based HE MGs are systematiclly investigated to further extend the δT_{FWHM} and obtain larger refrigeration capacity (RC) value in the past decades [8]. Among the new developed $Gd_{25}RE_{25}Co_{25}Al_{25}$ (RE = Tb, Dy, and Ho) [17], $Ho_{20}Er_{20}Co_{20}Al_{20}RE_{20}$ (RE = Gd, Dy, and Tm) [18], and $Gd_{10}Tb_{10}Dy_{10}Ho_{10}Er_{10}Y_{10}Ni_{10}Co_{10}Ag_{10}Al_{10}$ [19] RE-basd HE MGs, the $Er_{20}Dy_{20}Co_{20}Al_{20}Tm_{20}$ manifests the largest $|\Delta S_M|$ up to 11.9 Jkg^{-1}K^{-1}, while $Gd_{25}Ho_{25}Co_{25}Al_{25}$ possesses the largest RC up to 626 Jkg^{-1}. The outstanding magnetcaloric properties of these HE MGs may be ascribed to the high degree of the topological and chemical disorder based on the high mixing entropy in these HE MGs [17,20]. On the other hand, the HE effect also can enhance the thermal stability to improve the practicability of refrigerants during the cooling or freezing

* Corresponding authors.
E-mail addresses: yuanchenchenneu@hotmail.com, yuancc@seu.edu.cn (C.C. Yuan), blshen@seu.edu.cn (B.L. Shen).

https://doi.org/10.1016/j.jnoncrysol.2020.120354
Received 30 June 2020; Received in revised form 3 August 2020; Accepted 4 August 2020

cycling [21,22]. Therefore, it is valueable to take efforts on developing the RE-basd HE metallic refrigerants, such as $Gd_{25}Ho_{25}Co_{25}Al_{25}$ with both large $|\Delta S_M|$ and wide δT_{FWHM}. Additionally, the poor glass forming ability (GFA), high preparing cost, and settled T_C of the $Gd_{25}Ho_{25}Co_{25}Al_{25}$ restrains its practical application as refrigerants. Substituting Ho by other cheaper elements may reduce the cost and tune T_C in a wide temperature range, and still maintains large $|\Delta S_M|$ and RC values [23,24].

It is proposed that microalloying is an efficient method to improve the GFA, plasticity, soft magnetism, and magnetocaloric properties [25,26], which is beneficial for both crystalline and glassy refrigerants [5,24]. For example, substituting Ge with Fe of Gd-based crystalline alloy effectively reduces 90 percent of the magnetic hysteresis loss and still maintains large refrigeration capacity [5]. Besides, the adiabatic temperature change is improved by Zn addition, and T_C increases due to the substitution of Cd in Gd-based crystalline refrigerants [27]. For metallic refrigerant, the addition of Zr and Si effectively promotes the formation of $Gd_{55}Co_{20}Al_{25-x}Si_x$ and $Gd_{55}Co_{20}Fe_5Al_{20-x}Si_x$ (x = 0, 5, 10, 15) HE MGs due to the small size effect and restrained nucleation rate along with HE effect [23,24,26]. Meanwhile, substituting Al by Co in Gd–Co binary MGs also improves the GFA, $|\Delta S_M|$, and RC [28]. For the cheaper Y element, according to the work of Lu et al., the Y addition adjusts the compositions closer to the eutectic point thereby decreases liquidus temperatures and reduces the manufacturing obstacles by means of the formation of innocuous yttrium oxides [29,30]. As reported by Nabiałek et al. [31-33], the addition of Y decreases the intensity of magnetic susceptibility disaccommodation and increases the atomic packing density, which leads to the excellent soft magnetic properties of Fe-based MGs. The partial replacement of Nb by Y in the Fe-based and Gd-based bulk MGs is useful for achieving low coercivity and outstanding soft magnetic properties as well [34,35]. Moreover, the addition of Y as the high reserves of RE element can effectively tunes T_C and improves the GFA for the $Gd_{25}Co_{25}Al_{25}RE_{25}$ MG according to our previous work [36]. It is interesting to study the microalloying effect of Y addition on the thermodynamic and magnetocaloric properties of Gd-Co-Al-Ho HE MGs to obtain the optimum composition with the largest $|\Delta S_M|$ and GFA.

Based on the above considerations, we fabricate the $Gd_{25}Co_{25}Al_{25}Ho_{25-x}Y_x$ (x = 1, 5, 10, and 15) amorphous ribbons by melt-spinning method in this work. The infulence of Y addition on GFA, thermal stability, and magnetocaloric properties are investigated in detail. The possible association between δT_{FWHM} and $|\Delta S_M|$ is also discussed.

2. Experimental

The stoichiometric mixtures with nominal compositions of $Gd_{25}Co_{25}Al_{25}Ho_{25-x}Y_x$ (x = 1, 5, 10, and 15) were fabricated by arc melting high purity Gd, Co, Al, Ho, and Y, (above 99.9 wt.%) elements in Ti-gettered argon atmosphere. The ingots were re-melted four times to ensure the homogeneity of composition in alloys. Then small parts of ingots were cut, re-melted, and injected onto a spinning Cu roller with a linear speed of 40 m/s to prepare HE metallic ribbons. The width and thickness of the ribbons are of about 2 mm and 20 μm, respectively. The amorphous structure of the ribbons was confirmed by X-ray diffraction (XRD) with a Cu K_α radiation (2θ = 10 - 80°) and a scanning step is 0.02°, thus the time of exposing a sample to X-ray is about 8.75 min. Thermal analysis was carried out on differential scanning calorimeter (DSC) with a heating rate of 20 K/min by using glassy ribbons. The magnetic properties of samples were measured using a superconducting quantum interference device (SQUID) magnetometer (MPMS, Quantum Design) at the temperature range between 5 and 300 K. The magnetization isotherms were measured by step of 5 K near the magnetic transition temperature under the applied field of 5 T.

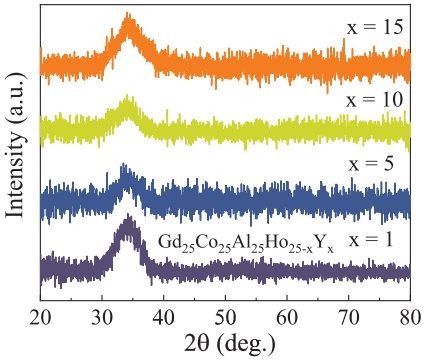

Fig. 1. XRD patterns of $Gd_{25}Co_{25}Al_{25}Ho_{25-x}Y_x$ (x = 1, 5, 10, and 15) HE metallic ribbons.

3. Results and discussion

Fig. 1 shows XRD patterns of the as-cast $Gd_{25}Co_{25}Al_{25}Ho_{25-x}Y_x$ (x = 1, 5, 10, and 15) ribbons. No pronounced crystalline peak appears in XRD curves and a typical board diffraction peak is observed, indicating the amorphous nature of the glassy ribbons. The DSC traces of $Gd_{25}Co_{25}Al_{25}Ho_{25-x}Y_x$ (x = 1, 5, 10, and 15) HE metallic ribbons are presented in Fig. 2. From the DSC traces, it can be seen that an endothermic glass transition peak occurs in these samples during the heating process, followed by several exothermic crystallization peaks, demonstrating a clear glass transition.

To evaluate the GFA of $Gd_{25}Co_{25}Al_{25}Ho_{25-x}Y_x$ (x = 1, 5, 10, and 15) MGs, the GFA criteria are calculated based on the thermal parameters that are obtained from DSC profiles, such as the glass transition temperature (T_g), the first crystalline temperature (T_x), the melting temperature (T_m), and the liquidus temperature (T_l). As listed in Table 1, the reduced glass-transition temperature T_{rg} ($T_{rg} = T_g/T_l$) [37], gamma parameters γ ($\gamma = T_x/(T_g+T_l)$), and γ_m ($\gamma_m = (2T_x-T_g)/T_l$) [38,39] show the largest values of about 0.61, 0.398, and 0.671, respectively, at the composition with x = 5. Hence, compared with the quaternary $Gd_{25}Co_{25}Al_{25}Ho_{25}$ MG [17], substituting 5 at.% Y element effectively improves the GFA. The outstanding GFA of Y-added MGs may be attributed to large differences in atomic size between the Y and other constituent elements in this multi-component system and the large negative heating of mixing [40].

The T_g, T_x, T_m, T_l, and supercooled liquid region ($\Delta T_x = T_x - T_g$) at the heating rate of 20 K/min are also listed in Table 1. The temperature dependence of T_g, T_x, and ΔT in $Gd_{25}Co_{25}Al_{25}Ho_{25-x}Y_x$ (x = 1, 5, 10, and 15) HE MGs is drawn in Fig. 3. Evidently, the T_g increases rapidly from 625 to 633 K as the content of Y increases from 1 to 5 at.%, and reaches the largest value of 633 K at x = 5, and then decreases to 628 K with further increasing the content of Y from 10 to 15 at.%. However, the T_x almost keeps constant of 664 K. Thus, the ΔT_x exhibits an

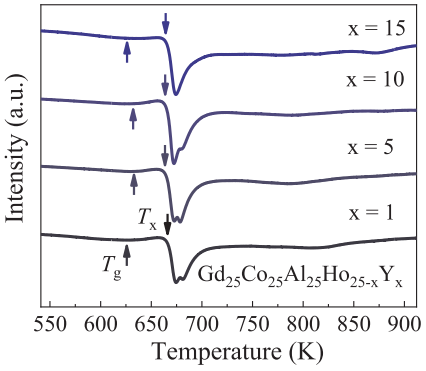

Fig. 2. DSC profiles of $Gd_{25}Co_{25}Al_{25}Ho_{25-x}Y_x$ (x = 1, 5, 10, and 15) HE metallic ribbons.

Table 1
The glass transition temperature T_g, first crystalline temperature T_x, supercooled liquid region ΔT_x, melting temperature T_m, liquidus temperature T_l, reduced glass-transition temperature T_{rg}, gama parameters γ and γ_m, and maximum magnetic entropy change $|\Delta S_{max}^{pk}|$ of $Gd_{25}Co_{25}Al_{25}Ho_{25-x}Y_x$ (x = 1, 5, 10, and 15) HE metallic ribbons under the external magnetic field of 5 T.

Composition	T_g (K)	T_x (K)	ΔT_x (K)	T_m (K)	T_l (K)	T_{rg}	γ	γ_m	$\lvert\Delta S_{max}^{pk}\rvert$ (J kg^{-1}K^{-1})	Ref.
$Gd_{25}Co_{25}Al_{25}Ho_{24}Y_1$	625.2	664	38.8	979	1058	0.59	0.395	0.665	8.63	This work
$Gd_{25}Co_{25}Al_{25}Ho_{20}Y_5$	633.3	664	30.7	982	1035	0.61	0.398	0.671	8.79	This work
$Gd_{25}Co_{25}Al_{25}Ho_{15}Y_{10}$	631.7	664	32.3	981	1049	0.60	0.395	0.663	7.61	This work
$Gd_{25}Co_{25}Al_{25}Ho_{10}Y_{15}$	627.8	665	37.2	983	1074	0.58	0.391	0.654	7.35	This work
$Gd_{55}Co_{20}Al_{25}$	597	669	72						8.9	[23]
$Gd_{55}Co_{20}Al_{24}Si_1$	599	678	79						9.2	[23]
$Gd_{55}Co_{20}Al_{23}Si_2$	602	680	78						8.9	[23]
$Gd_{55}Co_{20}Al_{22}Si_3$	604	667	63						8.9	[23]
$Gd_{52.5}Co_{18.5}Al_{29}$	604	679	75						4.6 (2 T)	[26]
$Gd_{52.5}Co_{18.5}Al_{28}Zr_1$	604	685	81						4.7 (2 T)	[26]
$Gd_{52.5}Co_{18.5}Al_{27}Zr_2$	604	684	80						4.4 (2 T)	[26]

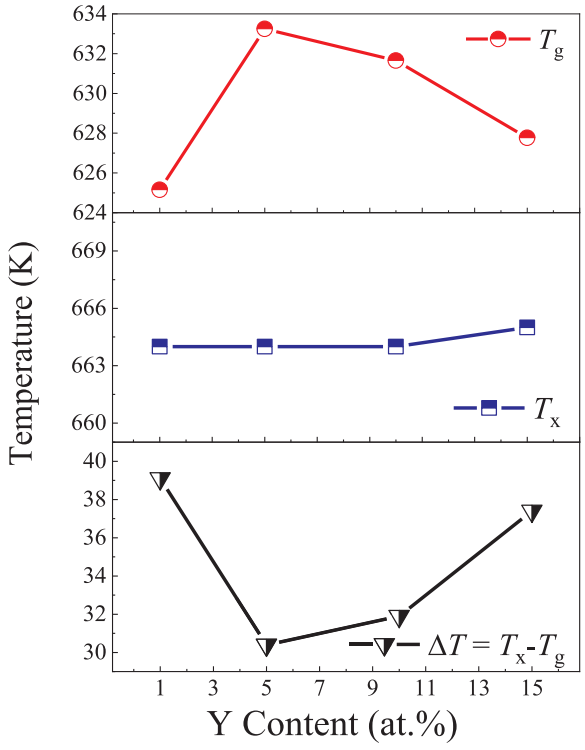

Fig. 3. T_g, T_x, and $\Delta T = T_x - T_g$ of $Gd_{25}Co_{25}Al_{25}Ho_{25-x}Y_x$ (x = 1, 5, 10, and 15) HE metallic ribbons as a function of Y content.

opposite changing trend as compared with T_g. For example, the ΔT_x of $Gd_{25}Co_{25}Al_{25}Ho_{24}Y_1$ is 38.8 K that is similar to the quaternary $Gd_{55}Co_{25}Al_{25}Y_{25}$ MG ($\Delta T_x \sim 36$ K [33]). Then it reaches the minimum value of 30.7 K at the composition with 5 at.% Y, and gradually increases to 37.2 K at x = 15. It is seen that the ΔT_x can be tuned from 30.7 to 38.8 K to improve thermal stability in a proper proportion by changing Y content in the Gd-Co-Al-Ho system. More interesting, differ from other Gd-based MG systems [23,41], $Gd_{25}Co_{25}Al_{25}Ho_{20}Y_5$ MGs with the most narrow supercooled liquid region exhibit the largest GFA among the studied $Gd_{25}Co_{25}Al_{25}Ho_{25-x}Y_x$ alloy system.

Fig. 4 presents the temperature dependence of the field cooling (FC) magnetization in $Gd_{25}Co_{25}Al_{25}Ho_{25-x}Y_x$ (x = 1, 5, 10, and 15) HE MGs under the applied magnetic field of 200 Oe. The field cooling curves were measured during the heating process after initial cooling from 300 to 5 K. Additionally, the magnetization of FC decreases and trends to zero with increasing the temperature, indicating the obvious magnetic phase transition from ferromagnetic to paramagnetic state. Meanwhile, the intensity of magnetization also decreases with the increase of Y

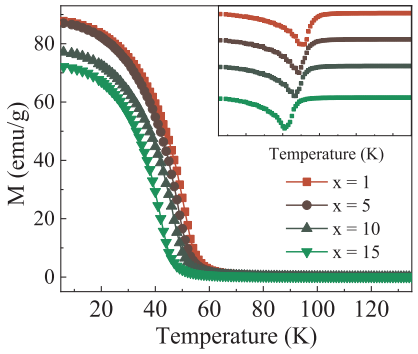

Fig. 4. Temperature dependence of the field cooling (FC) magnetization of the as-cast $Gd_{25}Co_{25}Al_{25}Ho_{20}Y_5$ HE metallic ribbons under the applied magnetic field of 200 Oe. The inset shows the dM/dT versus temperature curves.

content, which may be attributed to the decrease of magnetic exchange coupling in the amorphous phase [39,38]. The inset shows the dM/dT versus temperature curves. The T_C derived from dM/dT curves is 51, 49, 47, and 41 K for the composition with x = 1, 5, 10, and 15, respectively. Obviously, the values of T_C decrease with the increase of Y content. It demonstrates that replacing partial Ho with Y element restricts the magnetic interaction and leads to a relatively stronger thermal interaction effect to exhibit the lower T_C value of MGs.

The isothermal magnetization curves of the as-cast $Gd_{25}Co_{25}Al_{25}Ho_{20}Y_5$ HE ribbons are plotted in Fig. 5, which can be used to evaluate the MCE measured over a wide range of temperature between 10 and 120 K. Temperature intervals of 5 K for 40 - 80 K in the vicinity of T_C and 10 K for the regions far away from T_C such as 10 - 40 K and 80 - 120 K, respectively. The magnetization of the

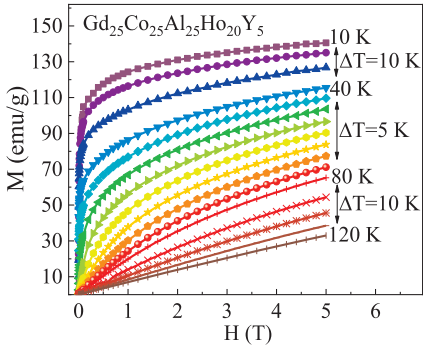

Fig. 5. The isothermal magnetization curves for the as-cast $Gd_{25}Co_{25}Al_{25}Ho_{20}Y_5$ HE metallic ribbons measured at the temperatures between 10 and 120 K. Temperature intervals of 5 K for 40 - 80 K and 10 K for 10 - 40 K and 80 - 120 K, respectively.

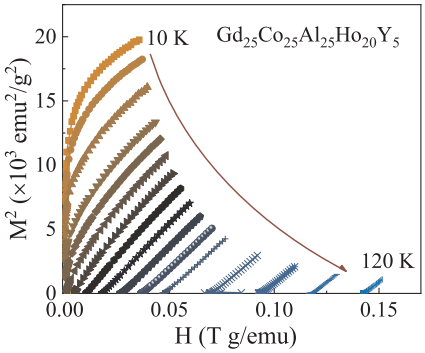

Fig. 6. The Arrott plots for $Gd_{25}Co_{25}Al_{25}Ho_{20}Y_5$ HE MGs measured at the temperature between the 10 and 120 K.

$Gd_{25}Co_{25}Al_{25}Ho_{20}Y_5$ HE MG increases abruptly and then slowly approaches to saturation at the temperature below T_C as a result of the ferromagnetic behavior. However, the curves gradually change into straight lines with further increasing the temperature near and above T_C, indicating a trasition from ferromagnetic to paramagnetic behavior.

To further identify the type of magnetic phase transition, the Arrott plots of $Gd_{25}Co_{25}Al_{25}Ho_{20}Y_5$ HE MG are measured at the temperature between the 10 and 120 K as one can see clearly in Fig. 6. According to the Banerjee criterion [42], the type of a magnetic phase transition can be certained by the slope of Arrott plots. The first order magnetic phase transition will display a negative slope and a positive slope is supposed to be a second order phase transition. Plots with positive slopes of $Gd_{25}Co_{25}Al_{25}Ho_{20}Y_5$ demonstrates a second order magnetic phase transiton from ferromagnetism to paramagnetism.

The MCE of a magnetic refrigerant is mainly characterized by the $|\Delta S_M|$. Fig. 7 displays the $|\Delta S_M|$ as a function of the temperature under different applied magnetic fields for the alloy with a composition of $Gd_{25}Co_{25}Al_{25}Ho_{20}Y_5$, which can be calculated by intergrating the Maxwell relation [15] over the applied magnetic field:

$$|\Delta S_M| = \int_{H_{min}}^{H_{max}} \left(\frac{\partial M}{\partial T}\right) dH \quad (1)$$

where H_{min} and H_{max} represent the initial and final values of the applied magnetic field, respectively. The maximal and minimal values of the magnetic field are 5 and 0 T in this work. The $|\Delta S_M|$ increases with a larger applied magnetic field during the whole temperature range and the maximum value of $|\Delta S_M|$ ($|\Delta S_{max}^{pk}|$) up to 8.79 Jkg^{-1}K^{-1} for this sample. It is found that the $|\Delta S_{max}^{pk}|$ also shifts to higher temperature with increasing magnetic field, which may be ascribed to the change of the magnetic free energy [17].

The $|\Delta S_M|$ as a function of temperature in $Gd_{25}Co_{25}Al_{25}Ho_{25-x}Y_x$ (x = 1, 5, 10, and 15) HE MGs is shown in Fig. 8, which are measured under the applied field of 5 T. It is noticed that the values of $|\Delta S_{max}^{pk}|$ are

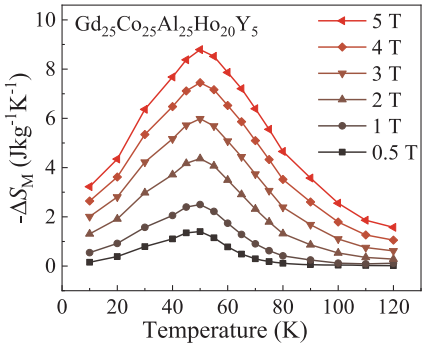

Fig. 7. Magnetic entropy changes ($-\Delta S_M$) versus temperature under the applied field of 0.5, 1, 2, 3, 4, and 5 T for $Gd_{25}Co_{25}Al_{25}$ $Ho_{20}Y_5$ HE MGs.

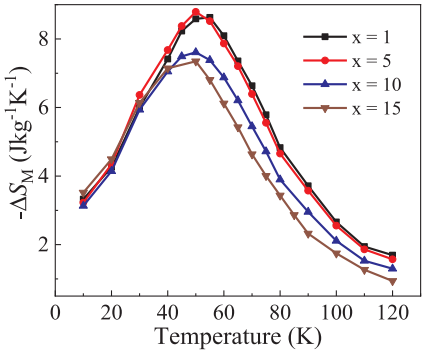

Fig. 8. Temperature dependence of magnetic entropy change ($-\Delta S_M$) in $Gd_{25}Co_{25}Al_{25}Ho_{25-x}Y_x$ (x = 1, 5, 10, and 15) HE MGs under the applied field of 5 T.

8.63, 8.79, 7.61, and 7.35 Jkg^{-1}K^{-1} when x = 1, 5, 10, and 15 for $Gd_{25}Co_{25}Al_{25}Ho_{25-x}Y_x$ HE MGs under an external magnetic field of 5 T, respectively, indicating a tunable $|\Delta S_M|$ by changing the content of Y element. On the other hands, the $|\Delta S_M|$ curves of these samples exhibit similar peaked shape with increasing temperatures.

The refrigeration capacity (RC) is another important parameter to evaluate magnetocaloric properties by the contrast of $|\Delta S_M|$. The value of RC can be calculated by Gschneidner's method [43]: RC = $|\Delta S_{max}^{pk}| \times \delta T_{FWHM}$, where δT_{FWHM} is the full width of half maximum of $|\Delta S_M|$. Under an external magnetic field of 5 T, the RC values are determined to be 555, 547, 490, and 488 J kg^{-1} for the compositions with x = 1, 5, 10, and 15, respectively. The magnetocaloric properties except for the $|\Delta S_{max}^{pk}|$ for these alloys are listed in Table 2.

The magnetic field variation of $|\Delta S_{max}^{pk}|$ and RC for the $Gd_{25}Co_{25}Al_{25}Ho_{25-x}Y_x$ (x = 1, 5, 10, and 15) HE MGs are shown in Fig. 9. One can find that the alloy of x = 5 has the largest $|\Delta S_{max}^{pk}|$ value under the applied field ranging from 0.5 to 5 T. The $Gd_{25}Co_{25}Al_{25}Ho_{24}Y_1$ exhibts the highest RC value up to 555 J kg^{-1}. Both $|\Delta S_{max}^{pk}|$ and RC have a clear correlation with the applied magnetic field [44]: $|\Delta S_{max}^{pk}| \propto H^n$ and RC $\propto H^N$. The exponents n and N, controlled by critical exponents of the alloy series, can be calculated by fitting the experimental data in Fig. 9(a-b) with the relation above. For all alloys x = 1, 5, and 10, n = 0.77; x = 15, n = 0.84. The exponents N are distinctive. For the alloy of x = 1, N = 1.05 ± 0.09, the alloy of x = 5, N = 1.03 ± 0.06, x = 10, N = 1.06 ± 0.09, and the alloy of x = 15, N = 1.13 ± 0.02, respectively. The exponent n near the T_C is similar to that of Fe-based (~0.75), Gd-based (~0.81), and Dy-based (~0.87) MGs, which deviates from the value of 2/3 corresponding to mean field theory [12,16,41]. The large n value likely originates from the existence of the local inhomogeneity, e.g., chemical short-range order, or impurities [45]. As listed in Table 2, the n values increase rapidly with increasing Y from 10 to 15 at.%. It is found that the composition with a larger amount of Y, for instance more than 10 at.% Y, exhibits larger n value, which may be due to the large local inhomogeneity existed in MGs.

The N is similar to that of $Gd_{25}Co_{25}Al_{25}Y_{15}Dy_{10}$ (~1.16) and $Ho_{20}Er_{20}Co_{20}Al_{20}Gd_{20}$ (~1.12), and $Gd_{25}Co_{25}Al_{25}Ho_{10}Y_{15}$ (~1.13) MGs, which is slightly larger than that of $Gd_{25}Co_{25}Al_{25}Y_{25}$ (~1.01) and $Gd_{25}Co_{25}Al_{25}Y_{15}Er_{10}$ (~1.03) MGs [33,16]. The larger N value may be attributed to the more drastic demagnetization effect [46]. Thus, the $Gd_{25}Co_{25}Al_{25}Ho_{20}Y_5$ MG with the smallest N value may exhibit the lowest demagnetization effect, which leads to the strongest magnetocloic response. This may be related to the largest value of $|\Delta S_{max}^{pk}|$ in this system. Among four studied MGs, the $Gd_{25}Co_{25}Al_{25}Ho_{10}Y_{15}$ MG exhibits the largest N value. It implies that RC of this alloy will increase more rapidly with increasing field that of other compositions, see Fig. 9(b). Therefore, according to the relation mentioned above, if the magnetic field is taken into consideration, the $Gd_{25}Co_{25}Al_{25}Ho_{10}Y_{15}$ alloy possesses more excellent magnetocaloric properties as a magnetic

Table 2
The magetocaloric properties except for the maximum magnetic entropy change $|\Delta S_{max}^{pk}|$ and configurational entropy ΔS_{config} for present $Gd_{25}Co_{25}Al_{25}Ho_{25-x}Y_x$ (x = 1, 5, 10, and 15) HE MGs under the external magnetic field of 5 T. The n and N are exponents of $|\Delta S_{max}^{pk}| \propto H^n$ and RC $\propto H^N$, and the R is gas constant (R = 8.314 $Jmol^{-1}K^{-1}$), respectively.

Composition	T_C (K)	δT_{FWHM} (K)	RC (J kg^{-1})	n	N	ΔS_{config}
x = 1	51	64.31	555	0.77 ± 0.007	1.05 ± 0.01	1.428R
x = 5	49	62.17	547	0.77 ± 0.006	1.04 ± 0.06	1.511R
x = 10	47	64.32	490	0.77 ± 0.007	1.06 ± 0.01	1.555R
x = 15	41	66.32	488	0.84 ± 0.002	1.13 ± 0.02	1.555R

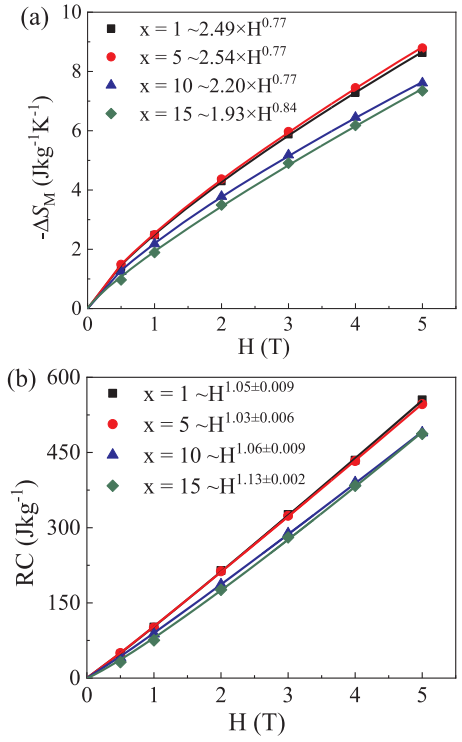

Fig. 9. The applied magnetic field as a function of the maximal values of magnetic entropy changes (– ΔS_M) (a) and RC (b) in $Gd_{25}Co_{25}Al_{25}Ho_{25-x}Y_x$ (x = 1, 5, 10, and 15) HE MGs. The solid lines are fitting curves of $|\Delta S_M| \propto H^n$ and RC $\propto H^N$ with standard errors.

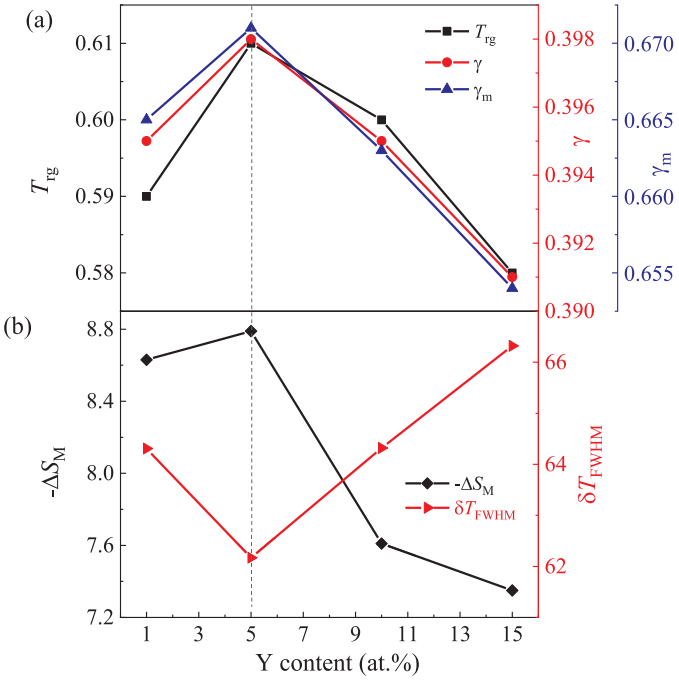

Fig. 10. The GFA criteria (a), δT_{FWHM} and $|\Delta S_M|$ (b) as a function of Y content in $Gd_{25}Co_{25}Al_{25}Ho_{25-x}Y_x$ (x = 1, 5, 10, and 15) HE MGs.

refrigerant at a higher magnetic field as compared with others.

The changing trends of the GFA criteria and magnetocaloric parameters with the increase of substituting elements for $Gd_{25}Co_{25}Al_{25}Ho_{25-x}Y_x$ (x = 1, 5, 10, and 15) RE-based MGs are displayed in Fig. 10(a-b). From Fig. 10(a), with the addition of Y, the GFA criteria such as T_{rg}, γ, and γ_m of $Gd_{25}Co_{25}Al_{25}Ho_{25-x}Y_x$ (x = 1, 5, 10, and 15) MGs increases from 0.59, 0.395, and 0.665 of $Gd_{25}Co_{25}Al_{25}Ho_{24}Y_1$ to 0.61, 0.398, and 0.671 of $Gd_{25}Co_{25}Al_{25}Ho_{20}Y_5$, respectively. The further addition of Y degrades the GFA and makes T_{rg}, γ, and γ_m decrease gradually down to much smaller values at the composition of $Gd_{25}Co_{25}Al_{25}Ho_{10}Y_{15}$. Therefore, the largest values of GFA criteria (T_{rg}, γ, and γ_m) and $|\Delta S_{max}^{pk}|$ are found at the same composition of $Gd_{25}Co_{25}Al_{25}Ho_{20}Y_5$ (Fig. 10(a-b)), indicating the best GFA and most excellent magnetocaloric properties can be achieved in this alloy system. Additionally, the ΔT exhibits an inverse composition dependence as compared with the $|\Delta S_{max}^{pk}|$ shown in Figs. 3 and 10(b). It demonstrates that the thermal parameters such as ΔT of MGs may be related to their magnetocaloric performance. This phenomenon has not been observed in other Gd-based MGs, such as $Gd_{55}Co_{20}Al_{25-x}Si_x$ (x = 0, 1, 2, and 3), $Gd_{55}Co_{20}Fe_5Al_{20-x}Si_x$ (x = 0, 5, 10, 15), and $Gd_{55}Co_{20-x}Al_{24}Si_1Fe_x$ (x = 0, 1, 2, 3, 4, and 5 at.%) MGs [23,24,38]. Nevertheless, this relationship may be conducive to predict the magnetocaloric properties of similar amorphous alloy systems.

By the study of the changing-trend curves of $|\Delta S_{max}^{pk}|$ in $Gd_{25}Co_{25}Al_{25}Ho_{25-x}Y_x$ (x = 1, 5, 10, and 15) MGs, both the Y content and the configurational entropy (ΔS_{config}) of magnetic elements (Gd, Co, and Ho) are the main factors that influence the magnetocaloric properties. On the basis of the previous study, we know that Y addition could affect the competition between the thermal effect and magnetic exchange interaction to tune the values of T_C. While the de Gennes factor of Y ion is zero, indicating that the Rare-Rare (R-R) exchange energy of Y element is near zero [47]. Therefore, the negligible yttrium moment results in less magnetic interactions between R-R elememts, thus leading to a smaller $|\Delta S_{max}^{pk}|$ value with increasing Y content in present MG systems. On the other hand, the ΔS_{config} is given by [48] $\Delta S_{config} = -R\sum_{i=1}^{n} X_i InX_i$, where n is the elements with configuration, X_i the mole fraction of i element, and R the gas constant: 8.314 $Jmol^{-1}K^{-1}$. The ΔS_{config} of magnetic elements (Gd, Co, and Ho) are 1.036 R, 1.015 R, 0.978 R, and 0.923 R, respectively. Whereas, the configurational entropy ΔS_{config} of all species of elements in the studied $Gd_{25}Co_{25}Al_{25}Ho_{25-x}Y_x$ systems are 1.428 R, 1.511 R, 1.555 R, and 1.555 R in $Gd_{25}Co_{25}Al_{25}Ho_{25-x}Y_x$ (x = 1, 5, 10, and 15) MGs, respectively. Following Boltzman's hypotheis on the relationship between entropy and system complexity [49], the ΔS_{config} of magnetic elements influences the spatial inhomogeneity of MGs and bonding state between magnetic atoms, which can also influence the magnetic interactions of the studied MG systems. The spatial inhomogeneity of real ferromagnetic materials is the origin of the off-set term in the maximum $|\Delta S_M|$ plotted against $H^{2/3}$, whose magnitude is proposed to be proportional to the value of δT_{FWHM} [50]. The composition with different δT_{FWHM} always leads to the variation of $|\Delta S_{max}^{pk}|$ in these MGs. As shown in

Fig. 10(b), the evolution of δT_{FWHM} as a function of Y content can be related to this fact. Therefore, the MG with lower spatial inhomogeneity and narrower δT_{FWHM} may exhibit a larger value of $|\Delta S_{max}^{pk}|$. Based on these factors, it can be concluded that the $Gd_{25}Co_{25}Al_{25}Ho_{20}Y_5$ sample exhibiting larger $|\Delta S_{max}^{pk}|$ than that of the compositions with less amount of Y addition like $Gd_{25}Co_{25}Al_{25}Ho_{24}Y_1$ may be attributed to the complex spatial inhomogeneity of Y-containing MGs corresponding to the large ΔS_{config}. On the other hand, the magnetic interactions as a dominant factor may reduce the values of $|\Delta S_{max}^{pk}|$ when the content of Y further increases. Therefore, $Gd_{25}Co_{25}Al_{25}Ho_{20}Y_5$ MG shows the largest value of $|\Delta S_{max}^{pk}|$ and lowest demagnetization effect according to the smallest exponent N as shown in Fig. 9(b).

4. Conclusions

In this work, the $Gd_{25}Co_{25}Al_{25}Ho_{25-x}Y_x$ (x = 1, 5, 10, and 15) MGs with outstanding MCE and low cost were fabricated by copper mold casting technology. The effect of Y substitution on the improvement of thermal and magnetocaloric properties as compared with quartary $Gd_{25}Co_{25}Al_{25}Ho_{25}$ MGs were investigated. The results can be concluded as follows:

(1) The addition of Y effectively improved the GFA of these alloys evaluated by the GFA criteria based on the thermal parameters. With 5 at.% Y addition, $Gd_{25}Co_{25}Al_{25}Ho_{20}Y_5$ MG exhibits the largest criteria value such as T_{rg} of 0.61, γ of 0.398, and γ_m of 0.671, indicating the best GFA of this MG system.
(2) The magnetization measurements showed that the T_C decreased from 51 to 41 K with the increase of Y content from 1 to 15 at.%, which may be attributed to the decrease of magnetic exchange coupling in the amorphous phase. Additionally, a non-linear relationship was displayed between the $|\Delta S_M|$ and Y content.
(3) Among these alloys, the $Gd_{25}Co_{25}Al_{25}Ho_{20}Y_5$ MG exhibited the largest value of $|\Delta S_{max}^{pk}|$ up to 8.79 J kg^{-1}K^{-1}, the minimum value of δT_{FWHM} up to 62.17 K, and a relatively higher RC up to 547 J kg^{-1} under the applied field of 5 T. This result could be attributed to multiple effects of the spatial inhomogeneity and magnetic interactions between R-R elememts. Such excellent MCE of Gd-Co-Al-Ho-Y HE MGs makes them attractive candidates for magnetic refrigerants.
(4) It is particular noting that the maximal $|\Delta S_M|$ and narrowest δT_{FWHM} were found in the same composition point of $Gd_{25}Co_{25}Al_{25}Ho_{20}Y_5$. Besides, the δT_{FWHM} also showed an inverse changing trend with respect to the $|\Delta S_M|$ with increasing Y content in $Gd_{25}Co_{25}Al_{25}Ho_{25-x}Y_x$ MGs, which may be ascribed to structural heterogenity and the demagnetization effect corresponding to the change of critical exponent N.

CRediT authorship contribution statement

C.M. Pang: Methodology, Software, Investigation, Data curation, Visualization, Writing - original draft. **C.C. Yuan:** Conceptualization, Investigation, Writing - original draft, Writing - review & editing, Project administration, Funding acquisition, Supervision. **L. Chen:** Investigation. **H. Xu:** Investigation. **K. Guo:** Investigation. **J.C. He:** Methodology, Software. **Y. Li:** Investigation. **M.S. Wei:** Methodology. **X.M. Wang:** Methodology, Writing - review & editing. **J.T. Huo:** Writing - review & editing. **B.L. Shen:** Writing - review & editing, Project administration, Funding acquisition.

Declaration of Competing Interest

None.

Acknowledgments

This work was supported by the National Natural Science Foundation of China (Grant Nos. 51631003 and 51601038), the Natural Science Foundation of Jiangsu Province, China (Grant No. BK20171354), the Fundamental Reasearch Funds for the Central Universities (Grant No. 2242020K40002), Jiangsu Key Laboratory for Advanced Metallic Materials (Grant No. BM2007204).

References

[1] K.A. Gschneidner, V.K. Pecharsky, Magnetocaloric materials, Annu. Rev. Mater. Sci. 30 (2000) 387–429.
[2] E. Warburg, Magnetische untersuchungen, Ann. Phys. 249 (1881) 141–164.
[3] V.K. Pecharsky, K.A. Gschneidner Jr, Giant Magnetocaloric Effect in $Gd_5(Si_2Ge_2)$, Phys. Rev. Lett. 78 (1997) 4494–4497.
[4] A.F. Lacaze, R. Beranger, G.B. Mardion, G. Claudet, A.A. Lacaze, Double acting reciprocating magnetic refrigerator: recent improvements, Adv. Cryog. Eng. (1984) 573–579 Springer.
[5] V. Provenzano, A.J. Shapiro, R.D. Shull, Reduction of hysteresis losses in the magnetic refrigerant $Gd_5Ge_2Si_2$ by the addition of iron (vol 429, pg 853, 2004), Nature 430 (2004) 810 -810.
[6] B.F. Yu, Q. Gao, B. Zhang, X.Z. Meng, Z. Chen, Review on research of room temperature magnetic refrigeration, Int. J. Refrig. 26 (2003) 622–636.
[7] C. Zimm, A. Jastrab, A. Sternberg, V. Pecharsky, K. Gschneidner, M. Osborne, I. Anderson, Description and performance of a near-room temperature magnetic refrigerator, in: P. Kittel (Ed.), Description and performance of a near-room temperature magnetic refrigerator, Adv. Cryog. Eng. 43 (Pts a and B) (1998) 1759–1766.
[8] V.K. Pecharsky, K.A. Gschneidner, Effect of alloying on the giant magnetocaloric effect of Gd-5(Si2Ge2), J. Magn. Magn Mater. 167 (1997) L179–L184.
[9] V.K. Pecharsky, K.A. Gschneidner, Magnetocaloric effect and magnetic refrigeration, J. Magn. Magn Mater. 200 (1999) 44–56.
[10] V. Franco, A. Conde, M.D. Kuz'min, J.M. Romero-Enrique, The magnetocaloric effect in materials with a second order phase transition: are T-C and T-peak necessarily coincident? J. Appl. Phys. 105 (2009) 07A917.
[11] F. Yuan, J. Du, B. Shen, Controllable spin-glass behavior and large magnetocaloric effect in Gd-Ni-Al bulk metallic glasses, Appl. Phys. Lett. 101 (2012) 032405.
[12] Q. Luo, D.Q. Zhao, M.X. Pan, W.H. Wang, Magnetocaloric effect in Gd-based bulk metallic glasses, Appl. Phys. Lett. 89 (2006) 081914.
[13] V.K. Pecharsky, K.A. Gschneidner, $Gd(Si_xGe_{1-x})(4)$: an extremum material, Adv. Mater. 13 (2001) 683–686.
[14] V.K. Pecharsky, K.A. Gschneidner, Magnetocaloric effect and magnetic refrigeration, J. Magn. Magn Mater. 200 (1999) 44–56.
[15] J. Du, Q. Zheng, Y.B. Li, Q. Zhang, D. Li, Z.D. Zhang, Large magnetocaloric effect and enhanced magnetic refrigeration in ternary Gd-based bulk metallic glasses, J. Appl. Phys. 103 (2008) 023918.
[16] J. Huo, L. Huo, J. Li, H. Men, X. Wang, A. Inoue, C. Chang, J.-.Q. Wang, R.-.W. Li, High-entropy bulk metallic glasses as promising magnetic refrigerants, J. Appl. Phys. 117 (2015) 073902.
[17] L. Xue, L. Shao, Q. Luo, B. Shen, GdRECoAl (RE = Tb, Dy and Ho) high-entropy glassy alloys with distinct spin-glass behavior and good magnetocaloric effect, J. Alloys Compd. 790 (2019) 633–639.
[18] Q. Luo, D.Q. Zhao, M.X. Pan, W.H. Wang, Magnetocaloric effect of Ho-, Dy-, and Er-based bulk metallic glasses in helium and hydrogen liquefaction temperature range, Appl. Phys. Lett. 90 (2007) 211903.
[19] J. Huo, J.-.Q. Wang, W.-.H. Wang, Denary high entropy metallic glass with large magnetocaloric effect, J. Alloys Compd. 776 (2019) 202–206.
[20] J. Huo, L. Huo, J. Li, H. Men, X. Wang, A. Inoue, C. Chang, J.-.Q. Wang, R.-.W. Li, High-entropy bulk metallic glasses as promising magnetic refrigerants, J. Appl. Phys. 117 (2015) 073902.
[21] S. Zhao, H. Wang, J. Gu, N. Guo, L. Shao, Y. Zhang, K. Yao, N. Chen, High strain rate sensitivity of hardness in Ti-Zr-Hf-Be-(Cu/Ni) high entropy bulk metallic glasses, J. Alloys Compd. 742 (2018) 312–317.
[22] S. Zhao, H. Wang, L. Xiao, N. Guo, D. Zhao, K. Yao, N. Chen, High strain rate sensitivity of hardness in quinary Ti-Zr-Hf-Cu-Ni high entropy metallic glass thin films, Physica E 94 (2017) 100–105.
[23] Q. Li, B. Shen, Glass-Forming Ability and Magnetocaloric Effect in $Gd_{55}Co_{20}Al_{25-x}Si_x$ Bulk Metallic Glass, Ieee T. Magn. 47 (2011) 2490–2493.
[24] H. Gencer, T. Izgi, V.S. Kolat, N. Bayri, A.O. Kaya, S. Atalay, The crystallisation kinetics, magnetic and magnetocaloric properties of $Gd_{55}Co_{20}Fe_5Al_{20-x}Si_x$ (x = 0, 5, 10, 15) alloys, J. Non-Cryst. Solids. 379 (2013) 185–191.
[25] X.-l. Hou, X. Jie, J. Huang, Z. Zeng, H.-m. Hu, G.-c. Zhang, H. Xu, Effect of B alloying on magnetocaloric effect of $Gd_{5.1}Si_2Ge_2$ alloy in low magnetic field, Prog. Nat. Sci. 21 (2011) 413–417.
[26] H. Fu, M. Zou, Y. Mudryk, V.K. Pecharsky, K.A. Gschneidner Jr., Enhancement of the glass-forming ability by Zr microalloying and its influence on the magnetocaloric properties of bulk amorphous Gd-Co-Al, J. Appl. Phys. 108 (2010) 053916.
[27] X. Wang, J. Bing, J. Wang, Q. Lu, X. Hou, H. Xu, Tunable magnetocaloric properties of Gd based alloys via Zn and Cd additions, Mater. Des. 134 (2017) 394–399.
[28] C. Wu, D. Ding, L. Xia, Effect of Al Addition on the Glass-Forming Ability and Magnetic Properties of a Gd-Co Binary Amorphous Alloy, Chin. Phys. Lett. 33

(2016) 016102.
[29] Z.P. Lu, C.T. Liu, W.D. Porter, Role of yttrium in glass formation of Fe-based bulk metallic glasses, Appl. Phys. Lett. 83 (2003) 2581–2583.
[30] S. Lu, S. Sun, K. Li, H. Li, X. Huang, G. Tu, The effect of Y addition on the crystallization behaviors of Zr-Cu-Ni-Al bulk metallic glasses, J. Alloys Compd. 799 (2019) 501–512.
[31] K. Sobczyk, J. Swierczek, J. Gondro, J. Zbroszczyk, W.H. Ciurzynska, J. Olszewski, P. Bragiel, A. Lukiewska, J. Rzacki, M. Nabialek, Microstructure and some magnetic properties of bulk amorphous $(Fe_{0.61}Co_{0.10}Zr_{0.025}Hf_{0.025}Ti_{0.02}W_{0.02}B_{0.20})_{(100-x)}Y_x$ (x = 0, 2, 3 or 4) alloys, J. Magn. Magn. Mater. 324 (2012) 540–549.
[32] M. Hasiak, K. Sobczyk, J. Zbroszczyk, W. Ciurzynska, J. Olszewski, M. Nabialek, J. Kaleta, J. Swierczek, A. Lukiewska, Some Magnetic Properties of Bulk Amorphous Fe-Co-Zr-Hf-Ti-W-B-(Y) Alloys, IEEE T. Magn. 44 (2008) 3879–3882.
[33] J. Gondro, K. Bloch, M. Nabialek, Structure and Magnetic Properties of Amorphous $Fe_{82}Zr_7Nb_2Cu_1B_8$ and Crystalline $Fe_{82}Zr_6Y_1Nb_2Cu_1B_8$ Alloys, Acta Phy. Pol. A 130 (2016) 909–912.
[34] T. Bitoh, D. Watanabe, Effect of Yttrium Addition on Glass-Forming Ability and Magnetic Properties of Fe-Co-B-Si-Nb Bulk Metallic Glass, Metals (Basel) 5 (2015) 1127–1135.
[35] J. Kastil, J. Kamarad, P. Javorsky, Magnetocaloric effect of $Gd_{64}Co_{26}Al_9Y_1$ metallic glass, J. Alloys Compd. 545 (2012) 1–4.
[36] C.M. Pang, L. Chen, H. Xu, W. Guo, Z.W. Lv, J.T. Huo, M.J. Cai, B.L. Shen, X.L. Wang, C.C. Yuan, Effect of Dy, Ho, and Er substitution on the magnetocaloric properties of Gd-Co-Al-Y high entropy bulk metallic glasses, J. Alloys Compd. 827 (2020) 154101.
[37] Z.P. Lu, H. Tan, Y. Li, S.C. Ng, The correlation between reduced glass transition temperature and glass forming ability of bulk metallic glasses, Scripta Mater. 42 (2000) 667–673.
[38] C.A. Angell, Formation of glasses form liquids and biopolymers, Science 267 (1995) 1924–1935.
[39] E.S. Park, W.T. Kim, D.H. Kim, The effect of in addition on the glass-forming ability in Cu-Ti-Zr-Ni-Si metallic glasses, Mater. Trans. 45 (2004) 2693–2696.
[40] A. Takeuchi, A. Inoue, Classification of bulk metallic glasses by atomic size difference, heat of mixing and period of constituent elements and its application to characterization of the main alloying element, Mater. Trans. 46 (2005) 2817–2829.
[41] L. Xue, J. Li, W. Yang, C. Yuan, B. Shen, Effect of Fe substitution on magnetocaloric effects and glass-forming ability in Gd-based metallic glasses, Intermetallics 93 (2018) 67–71.
[42] J. Fan, L. Ling, B. Hong, L. Zhang, L. Pi, Y. Zhang, Critical properties of the perovskite manganite $La_{0.1}Nd_{0.6}Sr_{0.3}MnO_3$, Phys. Rev. B 81 (2010) 144426.
[43] K.A. Gschneidner, V.K. Pecharsky, A.O. Pecharsky, C.B. Zimm, Recent developments in magnetic refrigeration, in: R.C. Woodward (Ed.), Rare Earths '98, 1999, pp. 69–76.
[44] V. Franco, J.S. Blazquez, A. Conde, Field dependence of the magnetocaloric effect in materials with a second order phase transition: a master curve for the magnetic entropy change, Appl. Phys. Lett. 89 (2006) 222512.
[45] L. Xue, Q. Luo, L. Shao, B. Shen, Magnetocaloric difference between ribbon and bulk shape of Gd-based metallic glasses, J. Magn. Magn Mater. 497 (2020) 166015.
[46] R. Caballero-Flores, V. Franco, A. Conde, L.F. Kiss, Influence of the demagnetizing field on the determination of the magnetocaloric effect from magnetization curves, J. Appl. Phys. 105 (2009) 07A919.
[47] J.F. Herbst, J.J. Croat, Magnetization of RFe_3 intermetallic compounds: molecular field theory analysis, J. Appl. Phys. 53 (1982) 4304–4308.
[48] J.W. Yeh, S.K. Chen, S.J. Lin, J.Y. Gan, T.S. Chin, T.T. Shun, C.H. Tsau, S.Y. Chang, Nanostructured high-entropy alloys with multiple principal elements: novel alloy design concepts and outcomes, Adv. Eng. Mater. 6 (2004) 299–303.
[49] R.A. Swalin, E. Burke, B. Chalmers, J.A. Krumhansl (Eds.), 2nd edn., Wiley, NY, 1991, p. 21.
[50] M.D. Kuz'min, M. Richter, A.M. Tishin, Field dependence of magnetic entropy change: whence comes an intercept? J. Magn. Magn Mater. 321 (2009) L1–L3.